Sensitivity and Specificity of Cetuximab-IRDye800CW to Identify Regional Metastatic Disease in Head and Neck Cancer

Rosenthal, Eben L.; Moore, Lindsay S.; Tipirneni, Kiranya; de Boer, Esther; Stevens, Todd M.; Hartman, Yolanda E.; Carroll, William R.; Zinn, Kurt R.; Warram, Jason M.

Published in:
Clinical Cancer Research

DOI:
10.1158/1078-0432.CCR-16-2968

Publication date:
2017

Published OnlineFirst April 26, 2017; DOI: 10.1158/1078-0432.CCR-16-2968

Personalized Medicine and Imaging

Clinical Cancer Research

Sensitivity and Specificity of Cetuximab-IRDye800CW to Identify Regional Metastatic Disease in Head and Neck Cancer

Eben L. Rosenthal[1], Lindsay S. Moore[2], Kiranya Tipirneni[3], Esther de Boer[4], Todd M. Stevens[5], Yolanda E. Hartman[2], William R. Carroll[2], Kurt R. Zinn[6], and Jason M. Warram[2]

Abstract

Purpose: Comprehensive cervical lymphadenectomy can be associated with significant morbidity and poor quality of life. This study evaluated the sensitivity and specificity of cetuximab-IRDye800CW to identify metastatic disease in patients with head and neck cancer.

Experimental Design: Consenting patients scheduled for curative resection were enrolled in a clinical trial to evaluate the safety and specificity of cetuximab-IRDye800CW. Patients ($n = 12$) received escalating doses of the study drug. Where indicated, cervical lymphadenectomy accompanied primary tumor resection, which occurred 3 to 7 days following intravenous infusion of cetuximab-IRDye800CW. All 471 dissected lymph nodes were imaged with a closed-field, near-infrared imaging device during gross processing of the fresh specimens. Intraoperative imaging of exposed neck levels was performed with an open-field fluorescence imaging device. Blinded assessments of the fluorescence data were compared to histopathology to calculate sensitivity, specificity, negative predictive value (NPV), and positive predictive value (PPV).

Results: Of the 35 nodes diagnosed pathologically positive, 34 were correctly identified with fluorescence imaging, yielding a sensitivity of 97.2%. Of the 435 pathologically negative nodes, 401 were correctly assessed using fluorescence imaging, yielding a specificity of 92.7%. The NPV was determined to be 99.7%, and the PPV was 50.7%. When 37 fluorescently false-positive nodes were sectioned deeper (1 mm) into their respective blocks, metastatic cancer was found in 8.1% of the recut nodal specimens, which altered staging in two of those cases.

Conclusions: Fluorescence imaging of lymph nodes after systemic cetuximab-IRDye800CW administration demonstrated high sensitivity and was capable of identifying additional positive nodes on deep sectioning. *Clin Cancer Res; 23(16); 4744–52. ©2017 AACR.*

Introduction

For many patients with head and neck squamous cell carcinoma (HNSCC), surgical resection with negative margins often constitutes primary or salvage treatment (1). Unfortunately, a significant portion of patients present with clinically and radiographically silent regional lymph node metastasis at the time of diagnosis (2, 3). The decision to undergo elective neck dissection at the time of initial extirpation is based on historical rates of occult metastatic disease. However, lymph node involvement remains an important factor in determining the appropriate staging and treatment plan (4), and is consistently associated with poor survival, particularly in patients with locally advanced HNSCC (3, 5–7). In fact, cervical lymph nodes are the most important site of recurrence for patients with oral cancer who did not undergo neck dissection at primary surgical resection (8). Although there are a number of factors to consider in the calculation of overall and disease-specific survival, a recent multivariate analysis demonstrated that lymph node metastasis represented the only significant independent prognostic indicator for all outcomes, including overall survival, disease-specific survival, and local recurrence in oral and oropharyngeal HNSCC (9).

For early-stage oral cancers, current National Comprehensive Cancer Network (NCCN) guidelines now recommend neck dissection or sentinel node biopsy at primary tumor resection irrespective of lymph node status (10), which was demonstrated in a recent study showing higher rates of overall and disease-free survival in patients undergoing elective neck dissection versus watchful waiting with therapeutic neck dissection (8). However, in cases of comprehensive neck dissection, the procedure can be associated with significant morbidity. Perhaps most commonly, shoulder dysfunction and pain occur after neck dissection due to accessory nerve injury (11–14). More specifically, 60% to 80% of patients undergoing a neck dissection with sectioning of the nerve have pain, limited abduction of the shoulder, and anatomic deformities, such as

[1]Department of Otolaryngology, Stanford University, Stanford, California. [2]Department of Otolaryngology, University of Alabama at Birmingham, Birmingham, Alabama. [3]Department of Surgery, University of Alabama at Birmingham, Birmingham, Alabama. [4]Department of Surgery, University Medical Center Groningen University of Groningen, Groningen, the Netherlands. [5]Department of Pathology, University of Alabama at Birmingham, Birmingham, Alabama. [6]Department of Radiology, University of Alabama at Birmingham, Birmingham, Alabama.

Note: Supplementary data for this article are available at Clinical Cancer Research Online (http://clincancerres.aacrjournals.org/).

Corresponding Author: Eben L. Rosenthal, Stanford University, Stanford, CA 94305. Phone: 650-723-4250; Fax: 650-723-2225; E-mail: ERosenthal@stanfordhealthcare.org

doi: 10.1158/1078-0432.CCR-16-2968

Published OnlineFirst April 26, 2017; DOI: 10.1158/1078-0432.CCR-16-2968

Translational Relevance

Lymph node metastasis remains the only significant independent prognostic indicator for all outcomes, including overall survival, disease-specific survival, and local recurrence. Furthermore, the accuracy of cancer staging directly determines the adjuvant treatment plan. For the first time, we demonstrate the potential of a systemically administered, cancer-targeting agent to molecularly image tumor-containing lymph nodes during surgery. Incorporating an intravenously delivered, cancer-specific agent to intraoperatively localize regional metastatic disease and improve staging accuracy represents an evolutionary leap in surgical diagnostics and treatment.

scapular flaring, droop, and protraction (15). The marginal mandibular nerve and the accessory nerve are often injured during neck dissection (16). Modified radical neck dissection and selective neck dissection are known to be associated with poor quality of life (17–19).

Fluorescence contrast-enhanced surgery has demonstrated promise in the detection of subclinical disease at the primary tumor (20). Although optical guided surgery has overcome the intrinsic limitations of the human eye to allow visualization of previously undetectable malignant tissue at the primary site, which may improve local control, the ability to detect regional lymphatics by tumor-specific probes has not been explored. Here, we show that development of tumor-specific fluorescence imaging has further ameliorated current deficits in oncologic surgery by extending tumor detection as it disseminates into regional lymph nodes. Interim results from a recent clinical trial (#NCT01987375) demonstrated that cetuximab-IRDye800CW could be safely administered as a tumor-specific contrast agent for use during surgical navigation to aid in the identification of subclinical disease with high sensitivity and specificity (21). It was determined that high levels of fluorescence, as measured by tumor-to-background ratio, correlated with primary HNSCC and may further represent a tumor-specific method for accurate detection of sentinel lymph node disease.

To that end, the current study seeks to evaluate the potential of cetuximab-IRDye800CW to identify metastatic disease in patients with head and neck cancer. The ability to specifically detect lymph node involvement is not simply limited to prognostic calculations; it represents a prodigious adjunct to current staging methods by accurately demonstrating the true stage of disease at the time of surgical resection and subsequently allowing for optimal adjuvant therapy. Similar to Methylene Blue Tc99m colloid, the approach may serve to provide the surgeon more accurate information at the time of surgery, thereby improving the precision of the dissection.

Materials and Methods

Study design

Patients scheduled to undergo surgical extirpation were identified in the otolaryngology clinic at the University of Alabama at Birmingham (Birmingham, AL). Patients were not enrolled if they had an allergic/infusion reaction to either a 10 or 100 mg test dose of unlabeled cetuximab. There were 14 individuals aged 40 to 84 years with biopsy-proven HNSCCs that were evaluated for trial eligibility; 2 patients experienced an infusion reaction to the test dose and were removed from the study, as reported previously (20). Karnofsky score of greater than 70%, and normal electrolyte parameters were required. All patients were given informed consent, and the UAB Institutional Review Board approved the study. The study was performed in accordance to the International Ethical Guidelines for Biomedical Research Involving Human Subjects (CIOMS). The FDA approved the study protocol (NCT01987375) and the manufacturing process of the cetuximab-IRDye800CW by the UAB Vector Production Facility as described previously (22). Sample size was based on traditional 3 + 3 phase I dose escalation model to identify the optimal tumor-to-background ratio. Consented patients meeting study criteria were admitted to the infusion center for study drug administration. A pretreatment dose of 10 or 100 mg unlabeled cetuximab was administered prior to the study drug to differentiate between a cetuximab reaction and a cetuximab-IRDye800CW reaction. During and after cetuximab-IRDye800CW infusion, hemodynamic measurements and ECG data were obtained. Safety and toxicity results, including adverse events, from the trial were reported previously (20). The escalating doses were based on the therapeutic dose of cetuximab (250 mg/m^2). The first 3 patients (cohort 1) were given a microdose (1% of therapeutic dose), cohort 2 received 10% of therapeutic dose, and cohort 3 received 25% therapeutic dose (Table 1). No outliers were excluded from the study analysis. All salivary glands were excluded from the study. To differentiate glandular tissue from lymphatic tissue, the salivary glands were removed from whole resected levels before imaging. The patients received the standard-of-care surgical and adjuvant treatment. The standard of care was maintained throughout the early-phase trial, which limits the utility of reporting follow-up data. When indicated, surgical resection of lymph nodes accompanied resection of the primary tumor 3 to 7 days following intravenous infusion of cetuximab-IRDye800CW. Patient characteristics with primary tumor site, cancer stage, and number of lymph nodes collected per cohort are shown in Table 1.

Cetuximab-IRDye800CW conjugation

Conjugation of cetuximab-IRDye800CW was performed under cGMP conditions, as described previously (22). Briefly, cetuximab (ImClone LLC, Eli Lilly and Company) was concentrated and pH adjusted by buffer exchange to a 10 mg/mL solution in 50 mmol/L potassium phosphate, pH 8.5. IRDye800CW NHS ester (LI-COR Biosciences) was conjugated to cetuximab for 2 hours at 20°C in the dark, at a molar ratio of 2.3:1. After column filtration to remove unconjugated dye and exchange buffer to PBS, pH 7, the final protein concentration adjusted to 2 mg/mL; the product was sterilized by filtration and placed into single-use vials and stored at 4°C until used.

Optical imaging

Open-field near-infrared imaging. Intraoperative imaging was performed pre-, inter-, and post whole neck dissection using an open-field optical imaging device (Luna Imaging System, Novadaq). Each resected neck level was also imaged *ex vivo* in the operating room using the open-field system modified with a black box stage. During open-field acquisition, video (10 s at 7.5 f/s and 1/4 s integration) of specimen in field of view (30 or 15 cm from camera) was collected at each time point. For qualitative analysis,

Published OnlineFirst April 26, 2017; DOI: 10.1158/1078-0432.CCR-16-2968

exported DICOMs were used to produce videos and images in the open-field device integrated instrument software (SPY-Q, Novadaq) using standardized threshold values.

Closed-field near-infrared imaging. The Pearl Impulse imaging platform (LI-COR Biosciences) was used to image fresh tissues obtained in the operating room prior to paraffin embedding. Whole resected neck levels were imaged intact prior to grossing. For cohort 1 (2.5 mg/m^2), there were 118 individual lymph nodes grossed and collected from neck levels in patient 1 (level 1–4), patient 2 (level 1–3), and patient 3 (level 1–4). For cohort 2 (25 mg/m^2), there were 197 total lymph nodes collected from patient 4 (level 1–4), patient 5 (level 1–4), patient 6 (level 2–4), patient 7 (level 2–5), patient 8 (level 2–4), and patient 9 (level 1–5). For cohort 3 (62.5 mg/m^2), there were 156 total lymph nodes collected from patient 10 (bilateral, 1–3), patient 11 (level 1–4), and patient 12 (bilateral, left 1–4, right 1–5). Grossed lymph nodes were imaging using the closed-field system prior to formalin fixation and paraffin embedding. The expected draining basin for each primary location was determined from the literature (23). For quantitative analysis, mean fluorescence intensity (MFI), defined as total counts/region of interest (ROI) pixel area, was calculated using custom ROI generated for each specimen using integrated instrument software (ImageStudio, LI-COR Biosciences). For determining the presence of disease by fluorescence, the blinded fluorescence assessment was performed qualitatively by the senior author using the onboard instrument software (ImageStudio, LI-COR Biosciences). For the assessment, the threshold was uniquely adjusted for each sample to reveal heterogeneity in fluorescence intensity within each sample, as described previously (24–26). Areas of high signal relative to the surrounding tissue were considered positive. Lymph nodes were given a binary assignment (±) determined by the presence or absence of tumor by each test. For the whole level analysis, the mean fluorescence values were calculated for each level by averaging the fluorescence values for each node collected for that corresponding level.

Histologic assessment

Grossed lymph nodes greater than 5 mm diameter were bisected prior to embedding, per standard of care. Sectioning of paraffin-embedded lymph nodes was performed using a cryotome. Blocks were sectioned into until full face thickness was achieved, at which point a section was mounted. A further section was mounted approximately 0.1 mm deeper to the first mounted section. Routine hematoxylin and eosin (H&E) staining was done for histologic assessment performed by a board-certified pathologist and then correlated with fluorescence intensity. The Odyssey imaging platform (LI-COR Biosciences) was used to determine fluorescence in slide-mounted sections obtained from paraffin-embedded blocks. IHC on unstained lymph node sections was performed to evaluate EGFR expression (anti-EGFR Ab-10, Thermo Fisher Scientific), tumor density (anti-pan-cytokeratin Ab-961, Abcam), and histiocyte presence (anti-CD68 ab31630 Abcam). Stained slides were imaged using the Bioimagene (Ventana Medical Systems) optical scanner. For the recut assessment, an additional section was obtained from 37 paraffin-embedded lymph nodes originally scored as false positive. The additional sections were collected approximately 1 mm into the cut face of each paraffin-embedded block. To control for chance sample error, control sections were similarly obtained from 37 paraffin-embedded lymph nodes originally scored as true negative. All recut sections were deidentified and subsequently assessed by a blinded board-certified pathologist.

Statistical analysis

Statistical comparisons were performed using Minitab 15 statistical software. Comparison of MFI was performed with a two-sided Wilcoxon and *t* tests to test for pairwise differences between sample types within each dose cohort. A *P* value of less than 0.05 was considered significant.

Results

Cetuximab-IRDye800CW localizes regional metastasis in head and neck cancer

During the trial, 12 patients received intravenous infusion of cetuximab-IRDye800CW 3 to 7 days prior to surgical resection of lymph nodes accompanied by primary tumor resection. To assess the specificity of the study drug for regional metastatic disease, *ex vivo* imaging using the closed-field device was performed on dissected lymph nodes, and results were compared with the diagnostic gold standard of histopathology. During resection and subsequent grossing of lymphatic levels, 471 total nodes were evaluated (Table 1). Closed-field fluorescence imaging resulted in 435 negative nodes, which were subsequently determined to be histopathologically negative

Table 1. Patient staging and lymph node distribution

				Pathology-positive lymph nodes		Pathology-negative lymph nodes		
Dose cohort	Patient number	Primary tumor site	Cancer stage	True positives	False negatives	False positives	True negatives	Patient total
Cohort 1 (2.5 mg/m^2)	1	Lateral tongue	T1, N2b	4	0	0	22	26
	2	Temple	T3, N0	0	0	1	59	59
	3	Floor of mouth	T3, N0	0	0	0	33	33
Cohort 2 (25.0 mg/m^2)	4	Floor of mouth	T4, N0	0	0	2	28	28
	5	Lateral tongue	T2, N1	1	1	0	48	50
	6	Lip	T0, N3	0	0	0	14	14
	7	Posterior neck	T2, N2b	7	0	0	44	51
	8	Piriform sinus	T1, N2b	16	0	0	20	36
	9	Hard palate	T4, N1	1	0	1	17	18
Cohort 3 (62.5 mg/m^2)	10	Septum	T2, N0	0	0	8	54	54
	11	Tonsil	T2, N1	1	0	1	31	32
	12	Floor of mouth	T3, N2b	5	0	20	65	70
Subtotal/total lymph nodes				35	1	34	435	471

Published OnlineFirst April 26, 2017; DOI: 10.1158/1078-0432.CCR-16-2968

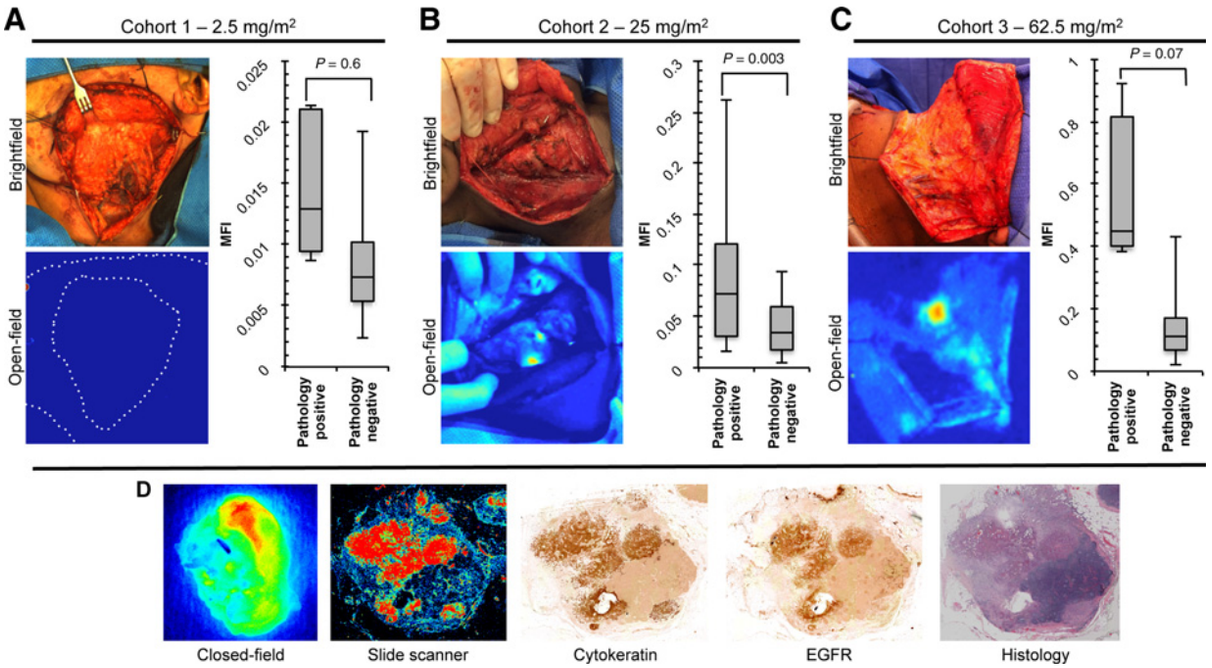

Figure 1.

Intraoperative imaging of neck dissection. Representative brightfield and open-field (Luna, Novadaq) images are shown along with quantitative analysis of grossed lymph node fluorescence for cohort 1–2.5 mg/m^2 dose group (**A**), cohort 2–25 mg/m^2 dose group (**B**), and cohort 3–62.5 mg/m^2 dose group (**C**). **D,** Representative closed-field (Pearl Impulse, LI-COR Biosciences) and fluorescence slide scanner (Odyssey, LI-COR Biosciences) acquisitions of grossed lymph node with adjacent IHC stains for cytokeratin and EGFR with matching histopathologic stain.

for disease (true negative). In addition, there were 35 true positive nodes (histology positive, fluorescence positive), 34 false-positive nodes (histology negative, fluorescence positive), and one false negative (histology positive, fluorescence negative).

For the microdose (2.5 mg/m^2) cohort, there was no identifiable contrast in the intraoperative and *ex vivo* setting (Fig. 1A) when the open-field imaging device was used. Quantitative analysis of images acquired using the closed-field device revealed an MFI of 0.015 ± 0.005 MFI for the pathology-positive nodes compared with 0.008 ± 0.003 MFI for the pathology-negative nodes ($P = 0.6$). In Supplementary Fig. S1A, representative closed-field acquisitions are shown for true-positive, false-positive, and true-negative gross lymph nodes from the 2.5 mg/m^2 dose cohort with accompanying fluorescence slide scanner imaging and adjacently sectioned H&E-stained specimens. In the 25 mg/m^2 dose cohort, focal areas of high fluorescence intensity were observed during open-field imaging (Supplementary Video S1) of intraoperative neck dissection and *ex vivo* imaging of whole resected levels (Fig. 1B). These areas were confirmed to be positive for metastatic disease (Supplementary Fig. S1B). Quantitative analysis (Fig. 1B) of images acquired using the closed-field device measured 0.084 ± 0.061 MFI for the pathology-positive nodes, which was significantly ($P = 0.003$) greater than 0.034 ± 0.022 MFI for the pathology-negative nodes.

In the highest dose cohort (62.5 mg/m^2), localized areas of high fluorescence intensity were observed during open-field, intraoperative imaging, and *ex vivo* imaging (Fig. 1C). Representative fluorescence imaging of grossly resected lymph nodes and adjacent H&E histologic stains from this dose cohort are shown in Supplementary Fig. S1C. Quantitative analysis (Fig. 1C) of images acquired using the closed-field device measured 0.590 ± 0.226 MFI for the pathology-positive nodes compared with 0.125 ± 0.071 MFI ($P = 0.07$) for the pathology-negative nodes. Figure 1D shows representative closed-field and fluorescence slide scanner acquisitions of grossed lymph node with adjacent IHC stains for cytokeratin (HNSCC marker) and EGFR with matching H&E. During analysis of closed-field acquisitions in this dose group, 29 false-positive lymph nodes were identified when compared with the gold standard of histology (Supplementary Fig. S1C). Further microscopic analysis revealed the majority of high-level fluorescence in these false-positive nodes occurred in areas of prominent sinus histiocytosis (Supplementary Fig. S2A), which was confirmed with CD68 staining (Supplementary Fig. S2B).

A single false negative was observed during the trial

During closed-field fluorescence acquisition of the grossed lymph nodes, a single false negative was observed in the 25 mg/m^2 dose cohort. In Fig. 2A, the closed-field and slide scanner fluorescence images with adjacent histologic H&E section are shown for this lymph node. Inset 10× digital zoom is also shown with adjacent IHC stains for cytokeratin and EGFR. Threshold-matched closed-field imaging of true-negative lymph nodes from the same patient are shown in Fig. 2B in addition to quantitative analysis for comparison of the false-negative lymph node (0.053 MFI) to pathology-positive (0.086 ± 0.062 MFI), pathology-negative (0.054 ± 0.062 MFI), and false-positive (0.054 ± 0.062 MFI) lymph node values from the same patient (Fig. 2C).

Published OnlineFirst April 26, 2017; DOI: 10.1158/1078-0432.CCR-16-2968

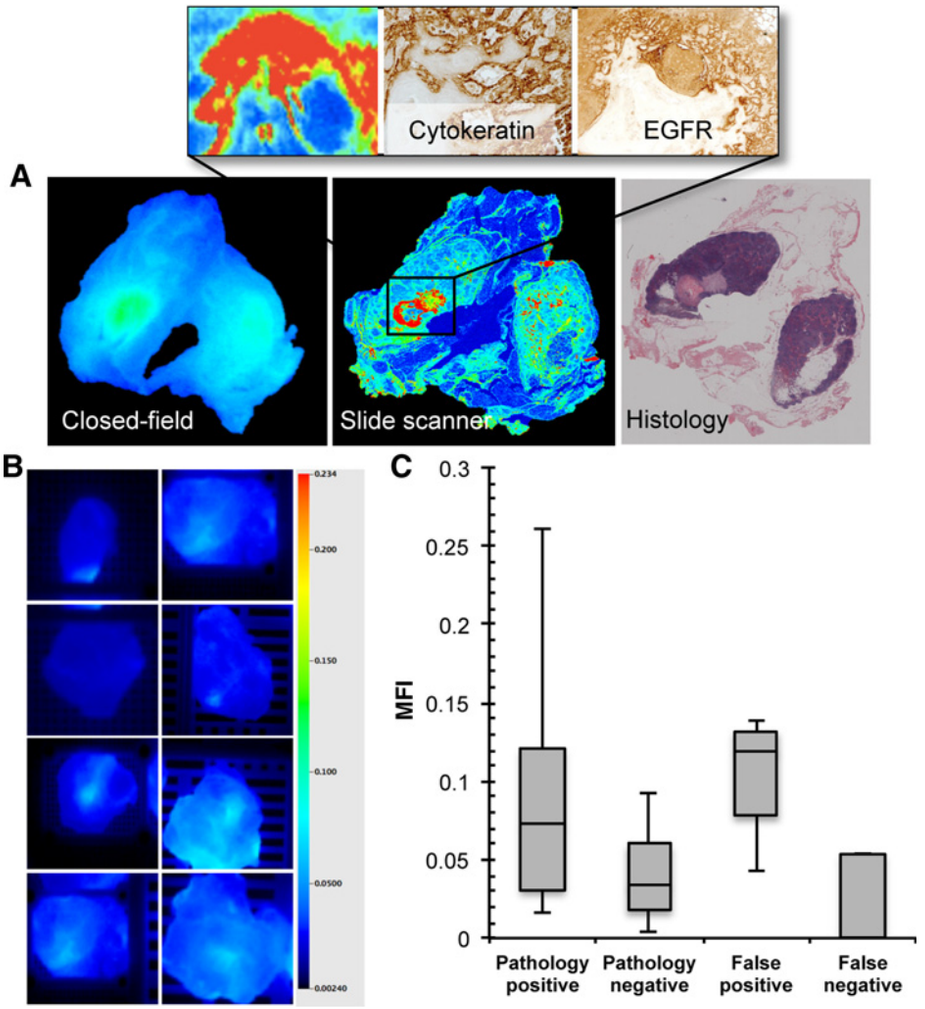

Figure 2.
Identification of single false-negative lymph node. **A,** Closed-field and slide scanner fluorescence images of false-negative (histology positive, fluorescence negative) lymph node with adjacent histologic H&E section and inset 10× digital zoom with adjacent IHC stains for cytokeratin and EGFR. **B,** Threshold-matched closed-field imaging of true-negative (histology negative, fluorescence negative) lymph nodes from the same patient. **C,** MFI of pathology-positive, pathology-negative, false-positive, and false-negative lymph nodes during closed-field acquisition.

Fluorescence imaging revealed misdiagnosis in 8.1% of false-positive lymph nodes

To ensure accurate diagnosis of the gold standard, an additional section was obtained from 37 paraffin-embedded lymph nodes originally scored as false positive. The additional sections were collected approximately 1 mm deep to the original section of each paraffin-embedded lymph node. To control for chance sample error, control sections were similarly obtained from 37 paraffin-embedded lymph nodes originally scored as true negative. During this additional analysis, three of 37 (8.1%) of the originally scored false-positive nodes, one node per dose cohort, were found to be positive for cancer by the blinded pathologist. In Fig. 3, a representative image of a true-positive (Fig. 3A) lymph node and originally scored false-positive (Fig. 3B) lymph node is shown with corresponding H&E stains. A 10× zoom of the originally scored histologic section from the false positive is shown in Fig. 3C with corresponding fluorescence slide scan. In Fig. 3D, the 1-mm deeper recut section is shown along with a 20× image highlighting a small focus of HNSCC cells that correlated with fluorescence areas on the slide scan acquisition. In two of those cases, the diagnosis of an additional metastatic lymph node would have significantly changed the adjuvant treatment plan for those patients. Importantly, there was no cancer found in the 37 recut, originally scored true-negative nodes.

Fluorescence imaging identified expected draining lymphatic level

During the study, analysis of mean fluorescence values from closed-field imaging of gross lymph nodes was used to examine the expected draining lymph node level, secondary level, and distal levels (Fig. 4A). For the 2 patients in the 2.5 mg/m^2 dose cohort with involved lymph nodes (Fig. 4B), the expected draining level for the lateral tongue tumor (level 2a, red font) was 0.021 MFI, which was higher than the average MFI of all other levels tested (0.01 MFI). For the 5 patients in the 25 mg/m^2 dose cohort (Fig. 4C) with involved nodes, the fluorescence of the expected draining level (0.091 ± 0.05 MFI) was greater than the secondary level (0.04 ± 0.02 MFI) and significantly ($P = 0.04$) greater than the distal levels (0.04 ± 0.01 MFI). A similar trend was also observed in the 62.5 mg/m^2 dose cohort (Fig. 4D), with greater fluorescence in the expected primary levels (0.24 ± 0.09 MFI) compared with the average from the other levels (secondary: 0.12 ± 0.06 MFI, distal:

Published OnlineFirst April 26, 2017; DOI: 10.1158/1078-0432.CCR-16-2968

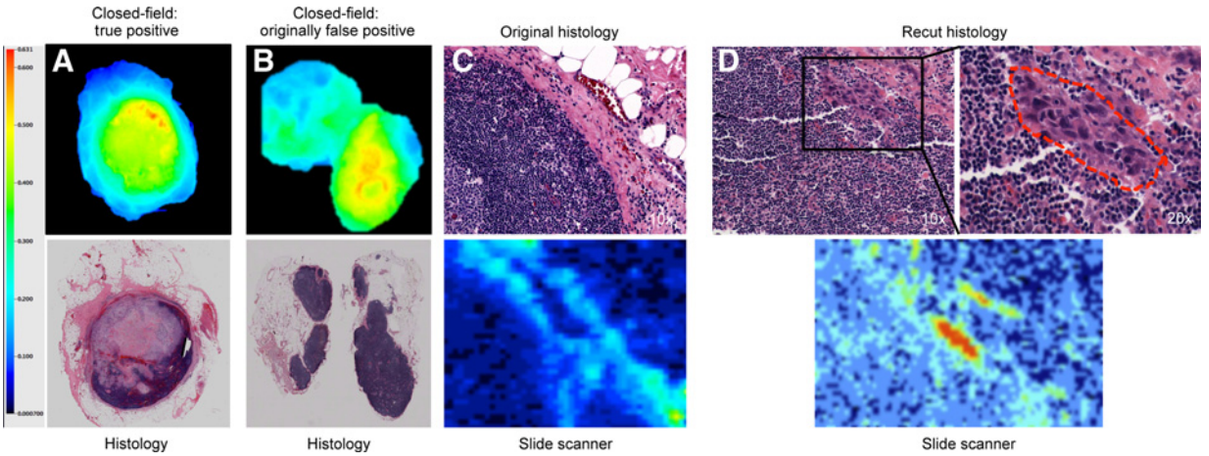

Figure 3.

Representative overturned case. **A,** Closed-field acquisition with matching histopathology of true-positive lymph node. **B** and **C,** Closed-field acquisition (**B**) with matching histopathology and fluorescence slide scanner acquisition (**C**) of fluorescent lymph node originally diagnosed as pathology negative. **D,** Histopathology and fluorescence slide scanner acquisition of deeper (1 mm) recut section with small focus of cancer.

0.14 ± 0.05 MFI). Patient 3 and 6 were true negative nodes only and are not shown. Overall, the fluorescence intensity in the expected drainage level was greater than all other levels for each patient.

Fluorescence imaging detected regional metastasis with high sensitivity and specificity

In Table 2, the overall statistics are shown for the 471 lymph nodes tested during the trial. The overall sensitivity was determined to be 97.2% due to the single false-negative and 435 true-negative lymph nodes, which translates to a negative predicative value of 99.7%. Similarly, the specificity was 92.7% for the 35 true-positive and 34 false-positive nodes. The high level of false-positive lymph nodes observed during the trial led to a positive predicative value of 50.7%.

Discussion

Here, we report the potential for systemically administered cetuximab-IRDye800CW to successfully identify regional metastatic disease in patients with HNSCC. During the trial, intraoperative imaging of excised lymphatic levels revealed areas of enhanced fluorescence *in situ* for the 25 mg/m^2 and 62.5 mg/m^2 dose groups. These levels were found to contain disease during histopathologic evaluation. In the microdose group (2.5 mg/m^2), closed-field imaging of grossly resected lymph nodes yielded the highest sensitivity (100%) and specificity (99.1%) for all doses. Despite this, the microdose was limited in identifying diseased nodes intraoperatively, which may be attributed to a limitation of the open-field device to detect trace amounts of cetuximab-IRDye800CW in these tissues. Limitations in fluorescence imaging were also seen with the highest dose cohort, where 85% of the false-positive lymph nodes were identified, leading to a poorer specificity (83.8%) for that dose. On the basis of *ex vivo* imaging results, the 25 mg/m^2 dose group generated the highest sensitivity (96.2%) and specificity (98.3%). Furthermore, this dose provided adequate contrast to identify positive lymph nodes *in situ* (Fig. 1), thus making this the optimal dose for both sensitive and specific guidance of diseased lymph node removal.

The wide variation in time intervals between study drug infusion and day of surgery (3–7 days) may have influenced the imaging results. The longer time interval may have adversely affected the tumor-specific fluorescence due to intracellular degradation leading to a "silencing" of the fluorescence signal. However, a shorter interval would suffer from high background signals producing a lower contrast value. The low number of patients along with the varying doses included in this study prohibits a thorough analysis of these timing effects. Future studies evaluating the optimal time to surgery are warranted to determine whether the strength of this application can be improved.

Initially, there were 37 false-positive nodes identified during the trial, which were fluorescently determined positive and histologically determined negative for disease on the final pathologic report. As part of the study, all 37 blocks of the false-positive nodes were sectioned deeper into the paraffin-embedded node. To account for chance sample error, 37 patient-matched true-negative nodes were also re-sectioned to a similar depth. Because of the amount of tissue remaining in the block and the need to retain adequate tissue for further clinical bearing, the tissue recut was only permitted to section 1 mm deeper into the block. This was a potential limitation to the recut analysis, as 1 mm is a relatively small amount of sampling considering many of these tissues were 5 mm to 1 cm in dimension. An additional limiting factor was the accuracy of histopathologic analysis, which is known to have discordance and sample error. The decision to use the gold standard of histopathology, rather than additional more accurate analysis, was based on the objective to measure the effectiveness of fluorescence imaging against the currently accepted standard of care. To make a comparison between fluorescence imaging and any nonclinically utilized assay would introduce an imbalanced comparison that would not be representative of current diagnostic standards. In addition, the number of patient-matched true negatives was chosen for reexamination to ensure that our additional analysis was not simply identifying errors in the gold standard nodal analysis. It is possible that there were additional nodes that were positive on rigorous serial

Published OnlineFirst April 26, 2017; DOI: 10.1158/1078-0432.CCR-16-2968

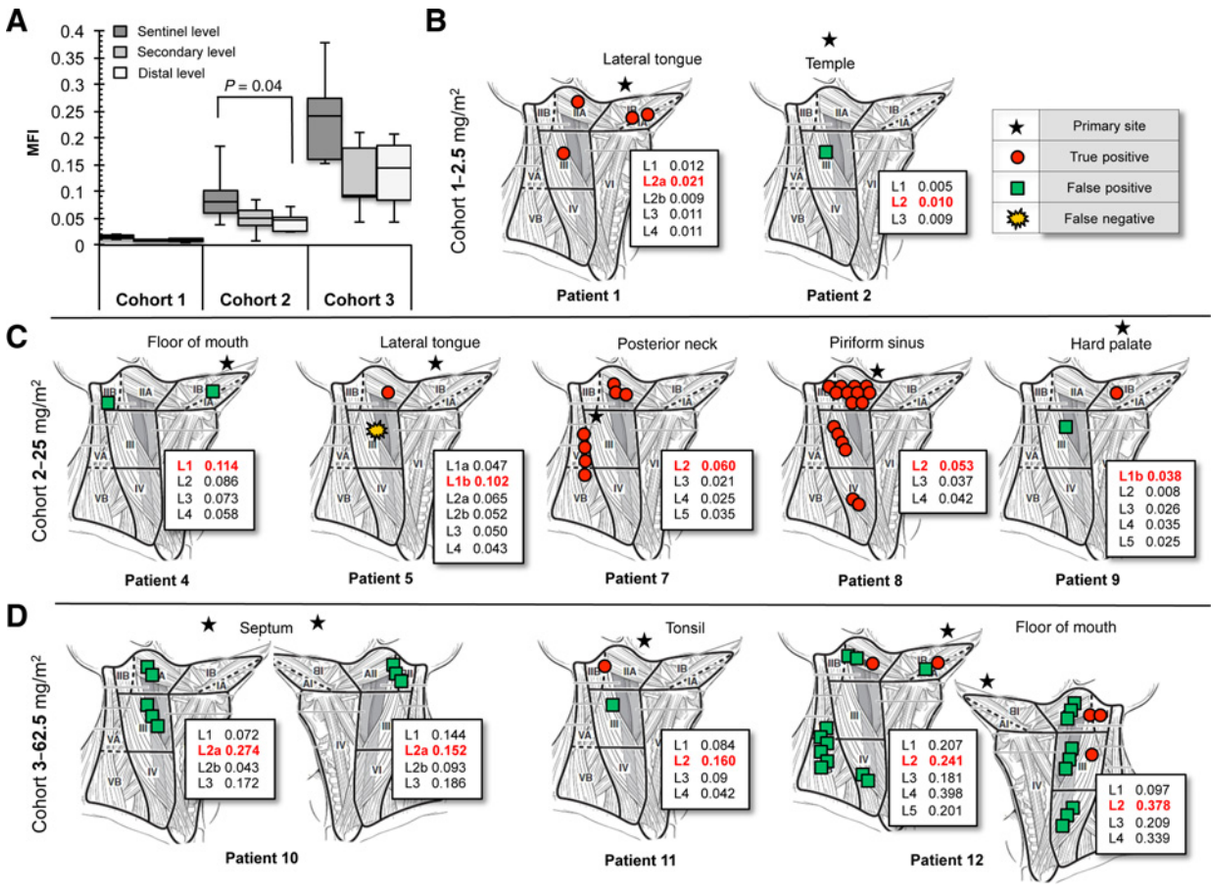

Figure 4.

Distribution of lymph nodes by level. **A,** Quantitative analysis from closed-field imaging of lymph nodes contained within the sentinel level, secondary level, and distal level for the 2.5 mg/m^2 (cohort 1), 25 mg/m^2 (cohort 2), and 62.5 mg/m^2 (cohort 3) dose groups. Illustrations of lymph node distribution per level with location of primary tumor for cohort 1 (**B**), cohort 2 (**C**), and cohort 3 (**D**). Inset values represent MFI for each level ("L") with red font indicating sentinel drain echelon for respective primary tumor location. Patient 3 and 6 contained true negatives only, not shown.

sectioning; therefore, our conclusions are limited to assessment on the limitations of current node-sectioning technique. Nevertheless, the additional sectioning revealed that 8.1% of the false-positive nodes were found to actually contain cancer, but there was no cancer discovered in the tissue blocks that were originally scored true-negative nodes. This significant discovery demonstrates the power of the utility in action. Perhaps most significantly, for two of the overturned cases, this new finding altered the staging of these patients, which may have changed the adjuvant treatment strategy.

Table 2. Cumulative statistics

Pathology positive	
True positive	35
False negative	1
Pathology negative	
False positive	34
True negative	435
Sensitivity	97.2%
Specificity	92.7%
Positive predictive value	50.7%
Negative predictive value	99.7%

Analysis of fluorescence slide scanner acquisitions from disease containing lymph nodes demonstrated the highly specific nature of cetuximab-IRDye800CW to localize cancer in these tissues. These results suggest that specific or targeted accumulation occurs in metastatic tumor cells harbored within lymph nodes. This would constitute specific targeting from the circulating vasculature. In addition, nonspecific lymphatic delivery was also evident from antibody–dye degradation products draining along lymphatic channels into the primary, secondary, and distal echelon nodes, which was measured by whole level fluorescence intensity. This could be considered similar to direct injection of sentinel node mapping agents, where antibody–dye bioconjugate collects in the primary tumor and then the degradation products drain nonspecifically through lymph nodes. Evidence for this mechanism was demonstrated with the high levels of fluorescence corresponding to areas of prominent sinus histiocytosis, which contains macrophages trafficking degradation products. It is difficult to speculate on future uses with such a limited sample, and future clinical trials should consider evaluating using this technique to limit the extent of elective cervical lymphadenopathy. However, it is possible that future improvements in agent selectivity

and imaging hardware may permit this technique to be used for highly selective neck dissections.

Collectively, these results suggest the potential use of fluorescence imaging to aid in the removal of subclinical positive nodes using cetuximab-IRDye800CW as a smart probe when used in combination with near-infrared (NIR) imaging. Competing strategies using lymphoscintigraphy or methylene blue rely on intratumoral administration followed by nonspecific drainage into primary echelon nodes. Here, cetuximab-IRDye800CW was shown to selectively target small foci of cancer cells contained within sentinel draining lymph nodes. This suggests a role for identification of sentinel levels for first echelon disease assessment using a disease-specific agent. The NIR properties of the IRDye800CW molecule would provide an additional advantage for sensitive fluorescence imaging due to the lower attenuation characteristics of fluorescence in this range.

Previously, we demonstrated this approach sensitive and specific to localize primary tumors for surgical guidance (20). Unlike direct injection techniques, systemic administration can be used for primary tumor removal, but also for identification of positive or at-risk lymph nodes. Importantly, a systemic agent could be used for the identification of primary echelon nodal basins and positive nodes beyond superficial tumors (breast, melanoma, oral cavity) to other tumors not amendable to direct injection, such as lung, colon, and prostate cancers. Finally, the use of radiolabeled antibodies administered systemically could be used for dual modality imaging using a PET tracer to improve preoperative PET imaging and intraoperative tumor localization. Combined with the current application for imaging regional metastasis, we have confirmed a multipurpose role of systemically injected cetuximab-IRDye800CW to improve surgical resection and staging in patients with head and neck cancer.

NCCN guidelines recommend a comprehensive neck dissection for biopsy-proven cervical metastasis, which can be associated with poor quality of life (11, 16, 27). Taken together, there is a persistent need for improved tumor-specific lymph node detection, particularly within the sentinel nodal basins, to decrease the incidence of unnecessary neck dissections and their associated morbidity. As such, the application of this technology has the potential to improve identification of cervical metastatic disease, which may improve outcomes in overall survival, disease-specific survival, and recurrence.

Disclosure of Potential Conflicts of Interest

No potential conflicts of interest were disclosed.

Authors' Contributions

Conception and design: E.L. Rosenthal, L.S. Moore, K. Tipirneni, K.R. Zinn, J.M. Warram

Development of methodology: E.L. Rosenthal, L.S. Moore, T.M. Stevens, K.R. Zinn, J.M. Warram

Acquisition of data (provided animals, acquired and managed patients, provided facilities, etc.): E.L. Rosenthal, L.S. Moore, K. Tipirneni, E. de Boer, T.M. Stevens, W.R. Carroll, J.M. Warram

Analysis and interpretation of data (e.g., statistical analysis, biostatistics, computational analysis): E.L. Rosenthal, L.S. Moore, E. de Boer, T.M. Stevens, K.R. Zinn, J.M. Warram

Writing, review, and/or revision of the manuscript: E.L. Rosenthal, L.S. Moore, K. Tipirneni, E. de Boer, T.M. Stevens, W.R. Carroll, K.R. Zinn, J.M. Warram

Administrative, technical, or material support (i.e., reporting or organizing data, constructing databases): L.S. Moore, E. de Boer, Y.E. Hartman, J.M. Warram

Study supervision: J.M. Warram

Acknowledgments

The authors acknowledge support from internal sources (Robert Armstrong Research Acceleration Fund), the UAB Comprehensive Cancer Center and NIH/NCI, and institutional equipment loans from Novadaq and LI-COR Biosciences.

Grant Support

This work was supported by grants from the NIH (R21CA182953, R21CA17917, T32CA091078), UAB Comprehensive Cancer Center, and Robert Armstrong Research Fund. Institutional equipment loans from LI-COR and Novadaq also supported this research. This work was also supported by grants R21CA182953 (to J.M. Warram, principal investigator), R21CA17917 (to E.L. Rosenthal, principal investigator), and T32CA091078 (to K. Bland, principal investigator).

The costs of publication of this article were defrayed in part by the payment of page charges. This article must therefore be hereby marked *advertisement* in accordance with 18 U.S.C. Section 1734 solely to indicate this fact.

Received November 29, 2016; revised January 26, 2017; accepted April 19, 2017; published OnlineFirst April 26, 2017.

References

1. Arbes SJ Jr, Olshan AF, Caplan DJ, Schoenbach VJ, Slade GD, Symons MJ. Factors contributing to the poorer survival of black Americans diagnosed with oral cancer (United States). Cancer Causes Control 1999;10:513–23.
2. Ozdek A, Sarac S, Akyol MU, Unal OF, Sungur A. Histopathological predictors of occult lymph node metastases in supraglottic squamous cell carcinomas. Eur Arch Otorhinolaryngol 2000;257:389–92.
3. Jemal A, Siegel R, Ward E, Hao Y, Xu J, Murray T, et al. Cancer statistics, 2008. CA Cancer J Clin 2008;58:71–96.
4. Leong SP, Cady B, Jablons DM, Garcia-Aguilar J, Reintgen D, Jakub J, et al. Clinical patterns of metastasis. Cancer Metastasis Rev 2006;25:221–32.
5. Howell GM, Grandis JR. Molecular mediators of metastasis in head and neck squamous cell carcinoma. Head Neck 2005;27:710–7.
6. Dunne AA, Muller HH, Eisele DW, Kessel K, Moll R, Werner JA. Meta-analysis of the prognostic significance of perinodal spread in head and neck squamous cell carcinomas (HNSCC) patients. Eur J Cancer 2006;42:1863–8.
7. Cady B. Lymph node metastases. Indicators, but not governors of survival. Arch Surg 1984;119:1067–72.
8. D'Cruz AK, Vaish R, Kapre N, Dandekar M, Gupta S, Hawaldar R, et al. Elective versus therapeutic neck dissection in node-negative oral cancer. N Engl J Med 2015;373:521–9.
9. Wong LS, McMahon J, Devine J, McLellan D, Thompson E, Farrow A, et al. Influence of close resection margins on local recurrence and disease-specific survival in oral and oropharyngeal carcinoma. Br J Oral Maxillofac Surg 2012;50:102–8.
10. National Comprehensive Cancer Network (NCCN). NCCN Clinical Practice Guidelines in Oncology: Head and Neck Cancers. Fort Washington, PA: National Comprehensive Cancer Network; 2016.
11. Bradley PJ, Ferlito A, Silver CE, Takes RP, Woolgar JA, Strojan P, et al. Neck treatment and shoulder morbidity: still a challenge. Head Neck 2011;33:1060–7.
12. Ebrahimi A, Zhang WJ, Gao K, Clark JR. Nodal yield and survival in oral squamous cancer: Defining the standard of care. Cancer 2011;117:2917–25.

Published OnlineFirst April 26, 2017; DOI: 10.1158/1078-0432.CCR-16-2968

13. de Bree R, Nieweg OE. The history of sentinel node biopsy in head and neck cancer: From visualization of lymphatic vessels to sentinel nodes. Oral Oncol 2015;51:819–23.
14. Hernando J, Villarreal P, Alvarez-Marcos F, Gallego L, Garcia-Consuegra L, Junquera L. Comparison of related complications: sentinel node biopsy versus elective neck dissection. Int J Oral Maxillofac Surg 2014;43:1307–12.
15. Shah S, Har-El G, Rosenfeld RM. Short-term and long-term quality of life after neck dissection. Head Neck 2001;23:954–61.
16. Gane EM, Michaleff ZA, Cottrell MA, McPhail SM, Hatton AL, Panizza BJ, et al. Prevalence, incidence, and risk factors for shoulder and neck dysfunction after neck dissection: a systematic review. Eur J Surg Oncol. 2016 Nov 17. pii: S0748-7983(16)30966-0. doi: 10.1016/j.ejso.2016.10.026. [Epub ahead of print]
17. Gil Z, Fliss DM. Contemporary management of head and neck cancers. Isr Med Assoc J 2009;11:296–300.
18. Malik A, Joshi P, Mishra A, Garg A, Mair M, Chakrabarti S, et al. Prospective study of the pattern of lymphatic metastasis in relation to the submandibular gland in patients with carcinoma of the oral cavity. Head Neck 2016;38:1703–7.
19. Nibu K, Ebihara Y, Ebihara M, Kawabata K, Onitsuka T, Fujii T, et al. Quality of life after neck dissection: a multicenter longitudinal study by the Japanese Clinical Study Group on Standardization of Treatment for Lymph Node Metastasis of Head and Neck Cancer. Int J Clin Oncol 2010;15:33–8.
20. Rosenthal EL, Warram JM, de Boer E, Chung TK, Korb ML, Brandwein-Gensler M, et al. Safety and tumor specificity of cetuximab-IRDye800 for surgical navigation in head and neck cancer. Clin Cancer Res 2015;21:3658–66.
21. Warram JM, de Boer E, Moore LS, Schmalbach CE, Withrow KP, Carroll WR, et al. A ratiometric threshold for determining presence of cancer during fluorescence-guided surgery. J Surg Oncol 2015;112:2–8.
22. Zinn KR, Korb M, Samuel S, Warram JM, Dion D, Killingsworth C, et al. IND-directed safety and biodistribution study of intravenously injected cetuximab-IRDye800 in cynomolgus macaques. Mol Imaging Biol 2015;17:49–57.
23. Mukherji SK, Armao D, Joshi VM. Cervical nodal metastases in squamous cell carcinoma of the head and neck: what to expect. Head Neck 2001;23:995–1005.
24. Day KE, Beck LN, Deep NL, Kovar J, Zinn KR, Rosenthal EL. Fluorescently labeled therapeutic antibodies for detection of microscopic melanoma. Laryngoscope 2013;123:2681–9.
25. Day KE, Beck LN, Heath CH, Huang CC, Zinn KR, Rosenthal EL. Identification of the optimal therapeutic antibody for fluorescent imaging of cutaneous squamous cell carcinoma. Cancer Biol Ther 2013;14:271–7.
26. Day KE, Sweeny L, Kulbersh B, Zinn KR, Rosenthal EL. Preclinical comparison of near-infrared-labeled cetuximab and panitumumab for optical imaging of head and neck squamous cell carcinoma. Mol Imaging Biol 2013;15:722–9.
27. Pinsolle V, Michelet V, Majoufre C, Caix P, Siberchicot F, Pinsolle J. [Spinal accessory nerve and lymphatic neck dissection]. Rev Stomatol Chir Maxillofac 1997;98:138–42.

Published OnlineFirst April 26, 2017; DOI: 10.1158/1078-0432.CCR-16-2968

Clinical Cancer Research

Sensitivity and Specificity of Cetuximab-IRDye800CW to Identify Regional Metastatic Disease in Head and Neck Cancer

Eben L. Rosenthal, Lindsay S. Moore, Kiranya Tipirneni, et al.

Clin Cancer Res 2017;23:4744-4752. Published OnlineFirst April 26, 2017.